VOL. 10, NO. 1, JANUARY 2015 ISSN 1819-6608
ARPN Journal of Engineering and Applied Sciences


www.arpnjournals.com

TRANSIENT-RATE ANALYSIS FOR HYDRAULICALLY-FRACTURED HORIZONTAL WELLS IN NATURALLY-FRACTURED SHALE GAS RESERVOIRS

Freddy Humberto Escobar[1], Juan Diego Rojas[1] and Alfredo Ghisays-Ruiz[2]
[1]Universidad Surcolombiana/CENIGAA, Avenida Pastrana, Neiva, Huila, Colombia
[2]Universidad del Atlántico, Fac. de Ciencias Básicas. antigua vía Puerto Colombia, Barranquilla, Atlántico, Colombia
E-Mail: fescobar@usco.edu.co

ABSTRACT

The actual energetic production is focused on searching for new supply sources which permit the constant-growing need of energy. This necessity and the depletion of conventional resources place as a goal the finding of such new oil resources as unconventional shale gas reservoirs. Then, an appropriate, accurate and practical way of characterizing these types of reservoirs is strongly needed and important for a better exploitation and managing of these fields. In this work new expressions are presented for rectangular geometry (slab) reservoirs using characteristic points found on the reciprocal-rate derivative vs. time log-log plot of tests run in such very low permeability formations as gas shales, based on the linear dual porosity model proposed by El-Banbi which describes the transient behavior of a hydraulically-fractured well in a shale gas formation. Equations were developed for estimating the fracture permeability the half-fracture length, the total matrix surface area draining into the fracture system, the interporosity flow parameter and the dimensionless storativity ratio. The equations were successfully tested with synthetic examples.

Keywords: fracture permeability, interporosity flow parameter, dimensionless storativity ratio, reciprocal-rate derivative, shale gas.

1. INTRODUCTION

We are currently inside the boom of unconventional reservoirs like those possessing micro-permeability (deposits of shale gas) and they are supplying considerable amounts of oil and gas, especially in the United States of America. Then, several studies have been devoted to understand both transient rate and pressure behavior of such systems.

Since shale gas systems are typically naturally-fractured, the initial studies must be addressed to that proposed by Warren and Root (1963) to describe a symmetric fractured network limited by cube matrix blocks.

Mayerhofer *et al.* (2006) presented a model for hydraulically-fractured well in a shale gas reservoir which represents the hydraulic fracture as an interconnected network of fractures. Their work indicates that drainage does not take place far beyond the stimulated region because of the low matrix permeability. This observation was also stated by Carlson and Mercer (1989).

Important contributions of transient behavior of shale gas formation have been lately formulated in the literature. Ozkan, Ohaeri and Raghavan (1987) presented details of five flow regimes taking place in fracture cylindrical reservoirs.

Watson *et al*. (1989) presented an analytical model for naturally-fractured reservoir with history matching. Their model accounted for variable gas properties. Another model for predicting production of a dewatered fracture coal shale gas formation was presented by Spivey and Semmelbeck (1995).

Brown *et al.* (2011) presented an analytical solution for a system with outer reservoir, inner reservoir, and the hydraulic fracture, and then couple the solutions with the flux- and pressure- continuity conditions on the interfaces between the regions and then inverted numerically from the Laplace space. Their mathematical model was used by Escobar, Bernal and Olaya-Marin (2014) to generate a practical methodology for interpretation of pressure tests in shale gas systems.

The most recent model presented in the literature for transient behavior of shale gas was presented by Fuente-Cruz, Gildin and Valko (2014). Fuentes-Cruz *et al*. (2014) modeled three cases of permeability variation: uniform (with no variation in permeability), linear and exponential. They used type-curve matching for the identification of the appropriate permeability model type which is dealt in a very different and more practical form in this work. It was found that, as expected, the uniform model has no permeability variations then the linear flow is followed by the pseudosteady-state regime. Escobar, Montenegro and Bernal (2014) applied the *TDS* methodology, Tiab (1993) for the interpretation of transient-rate tests using the model of Fuentes-Cruz *et al*. (2014).

El-Banbi (1998) presented a model for a hydraulically fractured horizontal shale gas well which was modeled as a horizontal well draining a rectangular geometry containing a network of fractures separated by matrix blocks (dual-porosity system). The solutions presented by El-Banbi (1998) for a linear dual porosity model will be applied to this system long with the analytical solutions proposed by Bello (2009). Bello (2009) presented a well-test interpretation methodology based upon straight-line conventional analysis.

2. MATHEMATICAL FORMULATION

2.1. Mathematical model

This study is based on analytical solutions proposed by Bello (2009) who used the linear dual porosity model proposed by El-Banbi (1998) to describe the hydraulically fractured shale gas reservoir system. This consisted of a bounded rectangular reservoir with slab matrix blocks draining into adjoining fractures and subsequently to a horizontal well in the center. The horizontal well fully penetrates the rectangular reservoir. The features of the El-Banbi model are described below:

- A closed rectangular geometry reservoir containing a network of natural and hydraulic fractures. The fractures do not drain beyond the boundaries of this rectangular geometry.
- The perforated length of the well, x_e, is the same as the width of the reservoir.
- Flow is towards the well at the center of the rectangular geometry.
- It is a dual porosity system consisting of matrix blocks and fractures.
- Both porous media are homogeneous and isotropic.
- Matrix acts as a uniformly distributed source for the fractures
- Fluid flows through the fractures to the wellbore.

2.2. Matrix (Slab) equations

The diffusivity equations for the matrix along with the initial and boundary conditions are given by:

$$\frac{\partial^2 p_{DLm}}{\partial z_D^2} = \frac{3}{\lambda_{Ac}}(1-\omega)\frac{\partial p_{Dm}}{\partial t_{DAc}} \tag{1}$$

Initial condition:

$$p_{DLm}(z_D, 0) = 0 \tag{2}$$

Inner boundary:

$$\left|\frac{\partial p_{DLm}}{\partial z_D}\right|_{z_D=0} = 0 \tag{3}$$

Outer boundary:

$$\left|p_{DLm}\right|_{Z_D=1} = p_{DLf} \tag{4}$$

Where λ_{Ac} and ω are given by:

$$\lambda_{Ac} = \frac{12}{L^2}\frac{k_m}{k_f}A_{cw} \tag{5}$$

$$\omega = \frac{(\phi c_t)_f}{(\phi c_t)_f + (\phi c_t)_m} \tag{6}$$

The dimensionless time and pressure variables are given for the slightly compressible fluid by:

$$t_{DAc} = \frac{0.0002637 k_f t}{(\phi\mu c_t)_{f+m} A_{cw}} \tag{7}$$

$$P_D = \frac{k_f\sqrt{A_{cw}}(P_i - P_{wf})}{141.2 q\beta\mu} \tag{8}$$

$$t_D * (P_D)' = \frac{k_f\sqrt{A_{cw}}(\Delta P)}{141.2 q\beta\mu} \tag{9}$$

And for the gas case by:

$$t_{DAc} = \frac{0.0002637 k_f t}{(\phi\mu c_t)_{f+m} A_{cw}} \tag{10}$$

$$m(P)_D = \frac{k_f\sqrt{A_{cw}}(m(P_i) - m(P_{wf}))}{1422 q_g T} \tag{11}$$

$$t_D * m(P_D)' = \frac{k_f\sqrt{A_{cw}}[t * \Delta m(P)']}{1422\ q_g T} \tag{12}$$

k_f is defined as the bulk fracture permeability.

2.3. Fracture equations

The diffusivity equations for the fracture and the initial and boundary conditions are given by:

$$\frac{\partial^2 p_{DLf}}{\partial y_D^2} = \omega\frac{\partial p_{DLf}}{\partial t_{DAc}} - \frac{\lambda_{Ac}}{3}\left|\frac{\partial p_{DLm}}{\partial z_D}\right|_{z_D=1} \tag{13}$$

Initial condition:

$$p_{DLf}(y_D, 0) = 0 \tag{14}$$

Inner boundary:

$$\left|\frac{\partial p_{DLf}}{\partial y_D}\right|_{y_D=0} = -2\pi \text{ (Constant rate)} \tag{15}$$

Outer boundary:

$$\frac{\partial p_{DLf}}{\partial y_D}\left(y_e/\sqrt{A_{cw}}, t_{DAc}\right) = 0 \text{ (No-flow boundary)} \tag{16}$$

2.4. Constant pressure inner boundary solution

The solution to the system presented by Bello (2009) in Equations (1) and (11) in the Laplace space is given by:

$$\overline{p_{wDL}} = \frac{2\pi}{s\sqrt{sf(s)}}\left[\frac{1+e^{-2\sqrt{sf(s)}y_{De}}}{1-e^{-2\sqrt{sf(s)}y_{De}}}\right] \quad (17)$$

Where

$$y_{De} = \frac{y_e}{\sqrt{A_{cw}}} \quad (18)$$

In Laplace space, the constant p_{wf} case at the wellbore can be found from the solution for the constant rate case given by Equation (15) using the Van Everdingen and Hurst (1949) relation given by Equation (17):

$$\overline{q_{DL}} = \frac{1}{s^2\overline{p_{wDL}}} \quad (19)$$

Equation (19) thus becomes for the constant p_{wf} case:

$$\frac{1}{\overline{q_{DL}}} = \frac{2\pi s}{\sqrt{sf(s)}}\left[\frac{1+e^{-2\sqrt{sf(s)}y_{De}}}{1-e^{-2\sqrt{sf(s)}y_{De}}}\right] \quad (20)$$

Equation (20) can then be inverted to obtain the solutions as a function of time using suitable Laplace numerical inversion algorithms such as Stehfest's inversion algorithm. The dimensionless variables are given for the gas case by:

$$t_{DAc} = \frac{0.0002637 k_f t}{(\phi\mu c_t)_{f+m} A_{cw}} \quad (21)$$

$$\frac{1}{q_D} = \frac{k_f\sqrt{A_{cw}}\left(m(P_i) - m(P_{wf})\right)}{1422 q_g T} \quad (22)$$

$$t_D * \left(\frac{1}{q_D}\right)' = \frac{k_f\sqrt{A_{cw}}[\Delta m(P)]}{1422 T}\left[t*(1/q)'\right] \quad (23)$$

2.5. TDS Formulation for reciprocal rate transient dual-porosity model

In this study an extension of the *TDS* technique, Tiab (1993), is presented in terms of the reciprocal-rate derivative based on the equations presented by Bello (2009) for each flow regime in the case of constant wellbore flowing pressure p_{wf}. New expressions taking into account the interception points between the different flow regimes are proposed. Equivalent equations are presented in Appendix A for the case of constant flow rate.

2.5.1. Early linear flow (Fractures)

The early linear flow has a slope of 0.5 in the reciprocal-rate derivative which reflects the single flow of fracture system; the matrix does not flow at early times.

As seen in Figure-1, the flow does not occur at small values of ω, this occurs because this parameter indicates the storage capacity of fractures, and if this is small, the fracures will not be able to affect the response of the reciprocal rate due to low fluid content.

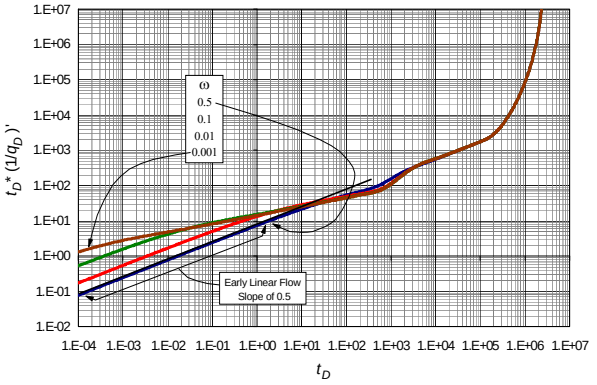

Figure-1. Effect storativity, ω, on the early linear flow under constant interporosity flow parameter, $\lambda_{Ac}=1\times10^{-3}$, and $y_{De}=1000$.

We can also see how that parameter ω does not affect the response at late times of the reciprocal rate at a particular dimensionless λ_{Ac}. According to the equations presented by Bello (2009) in a log-log plot of the dimensionless reciprocal flow versus dimensionless time, the initial flow regime is governed by the following expression:

$$q_{DL} = \frac{1}{2\pi\sqrt{\frac{\pi t_{DAc}}{\omega}}} \quad (24)$$

Inverting the flow rate and, then, taking the derivative with respect to time, it yields:

$$t_D*(1/q_{DL})' = \pi\sqrt{\frac{\pi t_{DAc}}{\omega}} \quad (25)$$

Once the dimensionless quantities given by Equations (21), (22) and (23) are replaced into Equation (25), it yields;

$$\frac{k_f\sqrt{A_{CW}}[\Delta m(P)]}{1422 T}\left[t*\left(\frac{1}{q}\right)'\right]_L = \pi\sqrt{\frac{\pi 0.0002637 k_f t_L}{\omega(\phi\mu c_t)_{f+m} A_{cw}}} \quad (26)$$

If the other parameters are known, Equation (26) allows calculating either the fracture permeability or the dimensionless storativity coefficient;

$$k_f = \frac{16533.277 t_L}{\omega(\phi\mu c_t)_{f+m}} \left(\frac{T}{A_{cw}\left[\Delta m(P)\right]\left[t*(1/q)'\right]_L} \right)^2 \quad (27)$$

$$\omega = \frac{16533.277 t_L}{k_f(\phi\mu c_t)_{f+m}} \left(\frac{T}{A_{cw}\left[\Delta m(P)\right]\left[t*(1/q)'\right]_L} \right)^2 \quad (28)$$

2.5.2. Bilinear flow regime

The bilinear flow regime is indicated by a one-fourth slope (0.25) of the reciprocal-rate derivative vs. time plot, see Figure-2. This flow regimen is caused by simultaneous transient flow in both fracture and matrix system.

It can be seenin Figure-2 that this flow regime occurs only in elongated reservoirs, that is, when length y_{De} (y_e/ [Acw] $^{0.5}$ > [3/λ_{Ac}] $^{0.5}$), otherwise, after the early linear flow regime, the matrix transient linear flow regime will be felt. This is because if the reservoir is not elongated, the flow in the fracture system is so short which does not allow the simultaneous flow to occur.

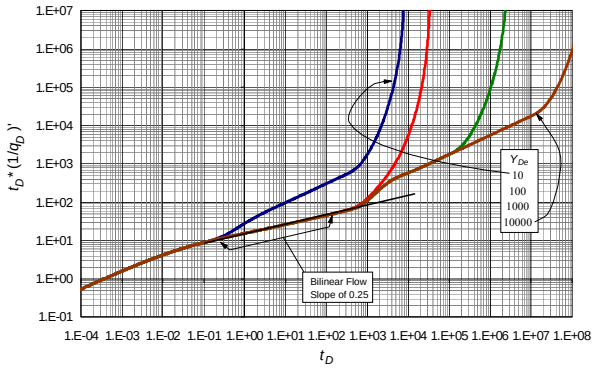

Figure-2. Effect the dimensionless reservoir length, y_{De}, on the bilinear flow regime under constant interporosity flow parameter, λ_{Ac}=1×10^{-3}, and dimensionless storativity ratio ω =1×10^{-2}.

However from observation of Figures 2 and 3, this flow regime is only function of the interporosity flow parameter, λ_{Ac}. Bello (2009) in a log-log plot of the dimensionless rate versus dimensionless time established that the bilinear flow regime is governed by the following equation:

$$q_{DBL} = \frac{\lambda_{Ac}^{0.25}}{10.133 t_{DAc}^{0.25}} \quad (29)$$

Applying the reciprocal rate and taking derivative with respect to time to the resulting equation, it yields,

$$t_D*(1/q_{DBL})' = \frac{10.133 t_{DAc}^{0.25}}{4\lambda_{Ac}^{0.25}} \quad (30)$$

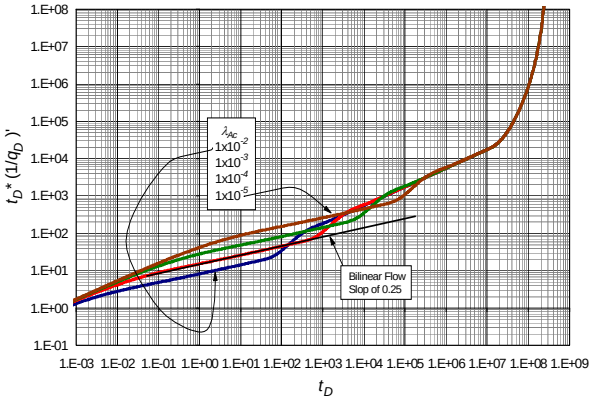

Figure-3. Effect the interporosity flow parameter, λ_{Ac}, on the bilinear flow regime under constant dimensionless reservoir length, y_{De} =1000, and dimensionless storativity ratio ω =1×10^{-2}.

Once the dimensionless quantities given by Equations (21), (22) and (23) are replaced into Equation (30), it yields;

$$\frac{k_f\sqrt{A_{CW}}\left[\Delta m(P)\right]}{1422T}\left[t*(1/q)'\right]_{BL} = \frac{10.133}{4}\left(\frac{0.0002637 k_f t_{BL}}{\lambda_{Ac}(\phi\mu c_t)_{f+m} A_{cw}} \right)^{0.25} \quad (31)$$

From which either fracture permeability or interporosity flow parameter can be solved for:

$$k_f = \left(\frac{459.045T}{\sqrt{A_{CW}}\left[\Delta m(P)\right]\left[t*(1/q)'\right]_{BL}} \right)^{1/0.75} \left(\frac{t_{BL}}{\lambda_{Ac}(\phi\mu c_t)_{f+m} A_{cw}} \right)^{1/3} \quad (32)$$

$$\lambda_{Ac} = \frac{t_{BL}}{k_f^3(\phi\mu c_t)_{f+m} A_{cw}} \left(\frac{459.045T}{\sqrt{A_{CW}}\left[\Delta m(P)\right]\left[t*(1/q)'\right]_{BL}} \right)^4 \quad (33)$$

2.5.3. Linear homogeneous flow

This flow regime occurs with a characteristics slope of 0.5 on the reciprocal-rate derivative vs. time plot similar to the early linear and matrix transient linear flow regimes. Unlike these, which are accompanied by other flow regimes, homogeneous linear flow regime is the only one that occurs throughout the test until pseudosteady state shows up. This behavior reflects the characteristics of a homogeneous reservoir, that is, there is no difference between the permeability of the fracture with the permeability of the matrix, presenting a single permeability.

It can be observed in Figure-4 that this homogeneous flow occurs when y_e/ [A_{cw}] $^{0.5}$> [3ω /λ_{Ac}] $^{0.5}$. For these conditions the reservoir behaves as one of the known homogeneous cases, when only one system is unique that contains or has the highest storage capacity of the fluid (in this case, when ω approaches 1).

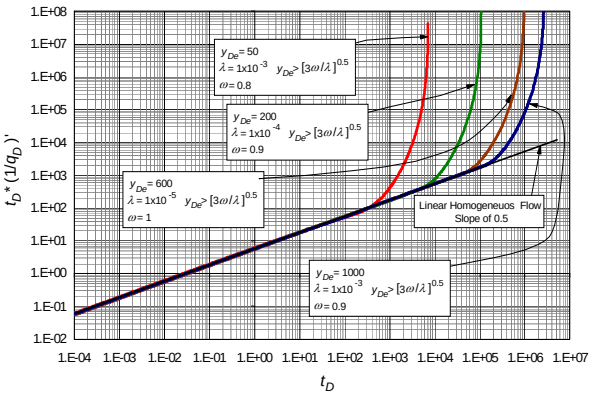

Figure-4. Effect the interporosity flow parameter, λ_{Ac}, storativity, ω, and dimensionless reservoir length, y_{De}, on linear homogeneuos flow regime.

For this linear homogeneous flow regime, the equation representing the behavior of the dimensionless rate versus dimensionless time presented by Bello (2009) is:

$$q_{DLh} = \frac{1}{2\pi\sqrt{\pi\, t_{DAch}}} \tag{34}$$

As for the former flow regimes, derivative is taken after inverting Equation (34) to obtain:

$$t_D * (1/q_{Dh})' = \pi\sqrt{\pi t_{DAch}} \tag{35}$$

Once the dimensionless quantities given by Equations (21), (22) and (23) are replaced into Equation (35), it yields;

$$\frac{k\sqrt{A_{cw}}\left[\Delta m(P)\right]}{1422T}\left[t*(1/q)'\right]_h = \pi\sqrt{\frac{\pi\, 0.0002637 k\, t_h}{(\phi\mu c_t)_{f+m} A_{cw}}} \tag{36}$$

From which the permeability of the homogeneous system is solved;

$$k = \left[\frac{128.5818T}{A_{cw}\left[\Delta m(P)\right]\left[t*(1/q)'\right]_h}\sqrt{\frac{t_h}{(\phi\mu c_t)_{f+m}}}\right]^2 \tag{37}$$

2.5.4. Matrix transient linear flow regime

In this flow, the behavior of dimensionless reciprocal rate is primarily the response from matrix drainage from the outer edges towards the matrix block center. A slope of 0.5 on the reciprocal-rate vs. time log-log plot.

This flow regime is shown in large (y_{De}) elongated fields as shown in Figure-5. Additionally, we can see how this flow regime is influenced by the interporosity flow parameter, λ_{Ac}, and dimensionless reservoir length, y_{De}.

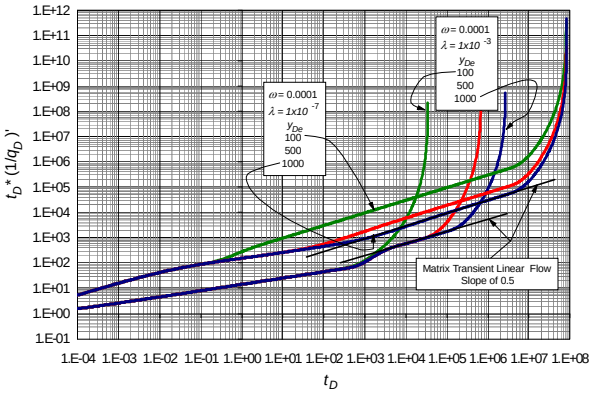

Figure-5. Effect the interporosity flow parameter, λ_{Ac}, and dimensionless reservoir length, y_{De}, to a constant dimensionless storativity ratio, ω=1×10^{-4}, during matrix transient linear flow regime.

Figure-5 shows two sets of curves with certain constant parameters. For relatively large values of the interporosity flow parameter (λ_{Ac}=1×10^{-3}), the variation of y_{De} affects only the duration of the matrix linear transient flow regime. For elongated reservoirs with large values of y_{De} this flow regime occurs for a longer test time. The starting time of this flow regime converges at the same point for different y_{De} values and it is the same in terms of location (no parallel displacement along the time axis).

Conversely, for small values of the interporosity flow parameter (λ_{Ac}=1×10^{-7}), the variation of y_{De} in addition to the effect of the duration of this flow regime generates that the starting time of this flow regime does not converge at the same point. It may occur to different times, generating a parallel displacement along the time axis.

Bello (2009) established the matrix transient linear flow govering equation:

$$q_{DLM} = \frac{1}{2\pi\sqrt{\pi\, t_{DAc}}}\sqrt{\frac{\lambda_{Ac}}{3}}\, y_{De} \tag{38}$$

Inverting the flow rate and then taking the derivative to the resulting equation will lead to obtain:

$$t_D * (1/q_{DLM})' = \frac{\pi\sqrt{3\pi}}{y_{De}}\sqrt{\frac{t_{DAc}}{\lambda_{Ac}}} \tag{39}$$

Once the dimensionless quantities given by Equations (21), (22) and (23) are replaced into Equation (39), it yields;

$$\frac{k_f\sqrt{A_{cw}}\left[\Delta m(P)\right]}{1422T}\left[t*(1/q)'\right]_{LM}=\frac{\pi\sqrt{3\pi}}{y_e}\sqrt{\frac{0.0002637k_f\,t_{LM}}{\lambda_{Ac}\left(\phi\mu c_t\right)_{f+m}}} \quad (40)$$

Either fracture permeability or interporosity flow parameter can be solved from Equation (40),

$$k_f=\frac{49599.831t_{Lm}}{A_{cw}\lambda_{Ac}\left(\phi\mu c_t\right)_{f+m}}\left[\frac{T}{y_e\left[\Delta m(P)\right]\left[t*(1/q)'\right]_{Lm}}\right]^2 \quad (41)$$

$$\lambda_{Ac}=\frac{49599.831t_{LM}}{k_f A_{cw}\left(\phi\mu c_t\right)_{f+m}}\left[\frac{T}{y_e\left[\Delta m(P)\right]\left[t*(1/q)'\right]_{LM}}\right]^2 \quad (42)$$

For this case (the slab matrix) and knowing that:

$$\lambda_{Acw}=\frac{12}{L^2}\frac{k_m}{k_f}A_{cw} \quad (43)$$

$$A_{cw}=\frac{L}{2y_e}A_{cm} \quad (44)$$

Equation (39) can be rewritten as:

$$q_{DLM}=\frac{1}{2\pi\sqrt{\pi\,t_{DAcm}}} \quad (45)$$

Applying the reciprocal rate and takin derivative to the resulting equation, it yields;

$$t_D*(1/q_{DLM})'=\pi\sqrt{\pi t_{DAcm}} \quad (46)$$

Once the dimensionless quantities given by Equations (21), (22) and (23) are replaced into Equation (46), it yields;

$$\frac{k_m\sqrt{A_{cm}}\left[\Delta m(P)\right]}{1422T}\left[t*(1/q)'\right]_{LM}=\pi\sqrt{\frac{\pi\,0.0002637k_m\,t_{LM}}{\left(\phi\mu c_t\right)_m A_{cm}}} \quad (47)$$

Solving for either the total matrix surface area draining or matrix permeability;

$$A_{cm}=\frac{128.5818T}{k_m\left[\Delta m(P)\right]\left[t*(1/q)'\right]_{LM}}\sqrt{\frac{k_m\,t_{LM}}{\left(\phi\mu c_t\right)_m}} \quad (48)$$

$$k_m=\frac{16533.2793t_{LM}}{\left(\phi\mu c_t\right)_m}\left[\frac{T}{A_{cm}\left[\Delta m(P)\right]\left[t*(1/q)'\right]_{LM}}\right]^2 \quad (49)$$

2.5.5. Pseudosteady-state period

This flow period represents the transient response of the reciprocal rate when the reservoir boundary begins influencing its behavior. Needless to remark that this flow period is normally recognized by a unit-slope straight line on a pressure test; however, during pseudosteady state of a transient reciprocal rate it does not follow unit-slope trend. Instead, constantly increasing curve is displayed; then, a tangent unit-slope line must be drawn on the derivative curve during this late time for the characterization of such regime. See Figure-6.

As seen in Figure-6, this flow period is not influenced by the interporosity flow parameter, λ_{Ac}, which affects only the time it occurs but not its characteristic equation. A uniform behavior was found by dividing the dimensionless time by the dimensionless squared reservoir length and the dimensionless reciprocal rate derivative by the dimensionless reservoir length, y_{De} for each case respectively.

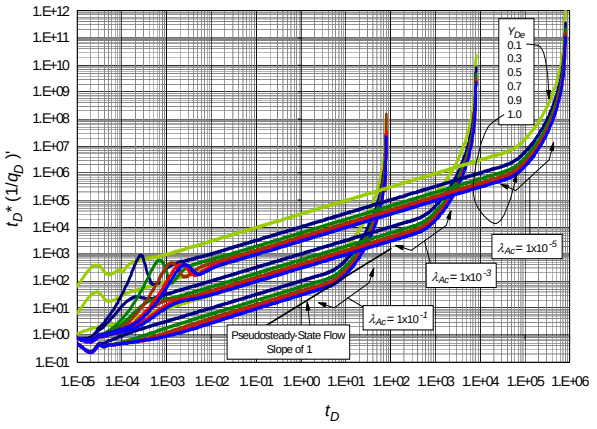

Figure-6. Effect the dimensionless reservoir length, y_{De}, to a constant storativity, $\omega = 0.01$, on Pseudosteady-State regime flow.

Once division is made, the dimensionless time and the dimensionless reciprocal rate derivative times y_{De}^2 and y_{De}, respectively, for each curve, the effect of the dimensionless reservoir length on the pseudosteady-state period can be seen in Figures-7 and 8. It can be observed as y_{De} changes the tangent points to the curve representing pseudosteady state period exhibits a linear behavior with unit slope. This linear behavior is independent of both the interporosity flow parameter, λ_{Ac}, and the dimensioness storativity ratio, ω. Figure-7 shows how these tangents points to the pseudostable State fall on the same line for different values of λ_{Ac},.

It can be seen in Figure-8 how the variation of the dimensionless storativity ratio, ω does not affect the behavior of the pseudosteady-state period. As mention earlier, this parameter affects only the early linear flow regime. Based on these observations, the governing equation during pseudosteady-state period is given by:

$$\frac{\left[t*(1/q_D)'\right]_{PSS}}{y_{De}}=4.76\pi\left(\frac{t_{DAc}}{y_{De}^2}\right)_{PSS} \quad (50)$$

Once the dimensionless quantities given by Equations (21), (22) and (23) are replaced into Equation (50), it yields;

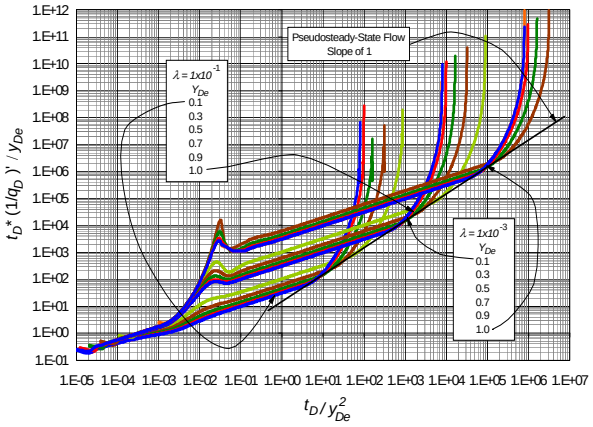

Figure-7. Effect the dimensionless reservoir length, y_{De}, to a constant storativity, $\omega = 0.01$, on Pseudosteady-State regime flow.

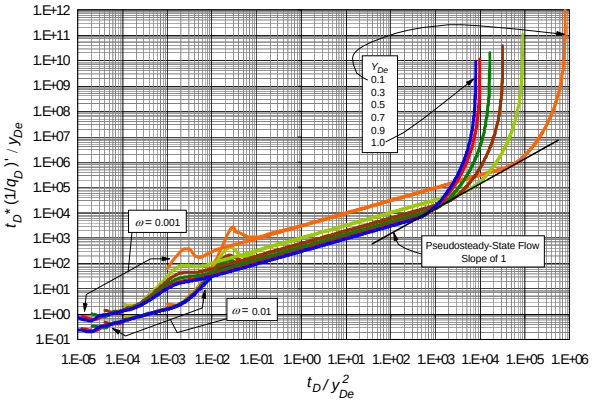

Figure-8. Effect the dimensionless reservoir length, y_{De}, to a constant interporosity flow parameter, $\lambda_{Ac} = 1\times10^{-3}$, on pseudosteady-state flow regime.

$$\frac{k_f\sqrt{A_{cw}}\left[\Delta m(P)\right]}{1422T}\left[t*(1/q)'\right]_{PSS} = \frac{4.76\pi\sqrt{A_{cw}}}{y_e}\left(\frac{0.0002637k_f\,t_{PSS}}{(\phi\mu c_t)_{f+m}\,A_{cw}}\right) \quad (51)$$

Solving for drainage half-length area from Equation (51), we obtain:tt

$$y_e = \frac{5.6075T\,t_{PSS}}{A_{cw}(\phi\mu c_t)_{f+m}\left[\Delta m(P)\right]\left[t*(1/q)'\right]_{PSS}} \quad (52)$$

Once y_e is calculated, then, the total matrix surface area draining in the fracture system can be estimated from:

$$A_{cm} = 2(y_e x_e) \quad (53)$$

2.5.6. Intersecting points

Based on the above-named flow regimes, the following new expressions are proposed for calculating the interporosity flow parameter, λ_{Ac} and the dimensionless storativity ratio, ω:

2.5.6.1. Early linear flow - bilinear flow

The intersection point formed by a drawn line on the early linear flow regime given by Equation (25) with the bilinear flow regime line given by Equation (30), t_{LBLi}, provides the following equation:

$$t_{DAc_{LBLi}}{}^{0.25} = \left(\frac{10.133}{4\pi}\right)\left(\frac{\omega}{\pi}\right)^{0.5}\left(\frac{1}{\lambda_{Ac}}\right)^{0.25} \quad (54)$$

Once the dimensionless quantities given by Equations (21), (22) and (23) are plugged into Equation (54), the storativity ω can be solved for:

$$\omega = 0.07846\left(\frac{k_f\,t_{LBLi}\,\lambda_{Ac}}{(\phi\mu c_t)_{f+m}\,A_{cw}}\right)^{0.5} \quad (55)$$

2.5.6.2. Bilinear flow - matrix transient linear flow:

The intersection point formed by the line of the bilinear flow regime, Equation (30), with the matrix transient linear flow regime line, Equation (39), t_{BLLMi}, gives,

$$t_{DAc_{BLLMi}}{}^{0.25} = \left(\frac{10.133\,y_{De}}{4\pi}\right)\left(\frac{1}{3\pi}\right)^{0.5}(\lambda_{Ac})^{0.25} \quad (56)$$

Once the dimensionless quantities given by Equations (21), (22) and (23) are plugged into Equation (56), the interporosity flow parameter λ_{Ac} can be solved for:

$$\lambda_{Ac} = \frac{0.05541\,A_{cw}k_f\,t_{BLLMi}}{y_e^4(\phi\mu c_t)_{f+m}} \quad (57)$$

2.5.6.3. Early linear flow - pseudosteady-state period:

The intersection point formed by the early linear flow regime straight line given by Equation (25) with the line of the pseudosteady-state period given by Equation (50), t_{LPSSi}, is given by the following equation:

$$t_{DAc_{LPSSi}}{}^{0.5} = \frac{y_{De}}{4.76}\sqrt{\frac{\pi}{\omega}} \quad (58)$$

Once the dimensionless quantities given by Equations (21), (22) and (23) are plugged into Equation (58), the storativity ω can be solved for:

$$\omega = 525.806 \frac{(\phi\mu c_t)_{f+m}\, y_e^2}{k_f\, t_{LPSSi}} \quad (59)$$

2.5.6.4. Bilinear flow - pseudosteady-state flow:

The intersection point formed by the bilinear flow regime straight line, Equation (30), with the pseudosteady-state period, Equation (50), t_{BLPSSi}, leads to,

$$t_{DAc_{BLPSSi}}{}^{0.75} = \frac{10.133 y_{De}}{4 \times 4.76 \pi \sqrt[4]{\lambda_{Ac}}} \quad (60)$$

Once the dimensionless quantities given by Equations (21), (22) and (23) are plugged into Equation (60), the storativity ω can be solved for:

$$\lambda_{Ac} = 44858022.57 A_{cw} y_e^4 \left(\frac{(\phi\mu c_t)_{f+m}}{k_f\, t_{BLPSSi}} \right)^3 \quad (61)$$

2.4.6.5. Matrix transient linear flow - pseudosteady-state flow:

Finally, the point of intersection resulting by a staright line drawn on the matrix transient linear flow regime given by Equation (39) with the pseudosteady-state flow period given by Equation (50), t_{LMPSSi}, provides the following expression:

$$t_{DAc_{LMPSSi}}{}^{0.5} = \frac{1}{4.76} \sqrt{\frac{3\pi}{\lambda_{Ac}}} \quad (62)$$

Once the dimensionless quantities given by Equations (21), (22) and (23) are plugged into Equation (62), and solving for the dimensionless storativity ratio ω, gives,

$$\lambda_{Ac} = \frac{1577.419 A_{cw} (\phi\mu c_t)_{f+m}}{k_f\, t_{LMPSSi}} \quad (63)$$

When bilinear flow regime, Matrix Transient Linear flow regimes and pseudosteady-state period are presented, Equations (60) and (62) can be combined to generate an additional expression allowing the calculation of fracture permeability regardless the presence of the interporosity parameter flow. This expression is:

$$k_f = 168.635\, y_e^2 (\phi\mu c_t)_{f+m} \sqrt{\frac{t_{LMPSSi}}{t_{BLPSSi}}} \quad (64)$$

A summary of the equivalent equations for the constant rate inner boundary case is also presented in Appendix-A.

3. EXAMPLES

Three examples are presented to verify the results obtained from the proposed expressions/technique. The first two corresponds to synthetic tests and the third correspond to a synthetic test developed by Bello (2009).

3.1. Example-1

The reciprocal rate and reciprocal rate derivative data for this test is provided in Figure-9 with the purpose of determining the permeability of fracture, the half-fracture length, the total matrix surface area draining into fracture system and the interporosity flow parameter. Other relevant data are given below:

q = 3 Mscf/D	ϕ = 30%	C = 0 bbl/psi
h = 100 ft	ω = 0.003	s = 0
X_e = 3000 ft	c_t = 1×10^{-4} psi-1	A_{cw}=6×10^5 ft^2
L = 50 ft	μ = 0.05 cp	
T = 720°R	$\Delta m(P)$ = 1.5×10^5 psi^2/cp	

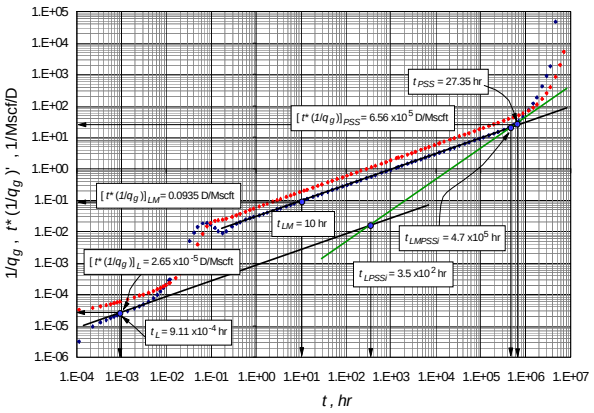

Figure-9. Log-log plot of the reciprocal rate and the reciprocal rate derivative vs. time for the Example-1.

Solution. The below parameters were read from Figure-9.

t_L = 9.11×10^{-4} hr	$[t^*(1/q_g)']_L$ = 2.65×10^{-5} D/Mscf
t_{LM} = 10 hr	$[t^*(1/q_g)']_{LM}$ = 0.0935 D/Mscf
t_{PSS} = 6.56×10^5 hr	$[t^*(1/q_g)']_{PSS}$ = 27.35 D/Mscf
t_{LPSSi} = 3.5×10^4 hr	
t_{MLPSSi} = 4.7×10^5 hr	

Due to reservoir conditions the bilinear flow regime does not occurs for that reason the equations generated for this flow regime are not used. However, with the given flow regimes all parameters can be estimated.

Initially, since fracture permeability is unknown, the half-fractures length is calculated by means of Equation (52) using the pseudosteady-state period, generating a value of y_e = 695.863 ft. With this value, of y_e, the total matrix surface area draining into the fracture system can be calculated by Equation (53) providing A_{cm} = 4175178 ft^2. Since ω = 0.003, the fracture permeability can be estimated using Equation (27), which result is k_f =

305.82 md. Finally, the interporosity flow parameter can be calculated with the point of interception between matrix Transient linear flow regime and pseudosteady-state period, Equation (63), which result is $\lambda_{Ac} = 9.88\times10^{-6}$. In order to compare results, λ_{Ac} and ω can be calculated with equations (42) and (59) respectively giving as results $\lambda_{Ac} = 9.81\times10^{-6}$ and $\omega = 3.57\times10^{-3}$. The input and calculated parameters are shown in Table-1.

Table-1. Summary of results for Example-1.

Parameter simulated		Parameter calculated		Eq.
y_e (ft)	697.137	y_e (ft)	695.863	52
A_{cm} (ft^2)	4182822.014	A_{cm} (ft^2)	4175178	53
k_f(md)	300	k_f(md)	305.82	27
ω	0.003	ω	3.57×10^{-3}	59
λ_{Ac}	1×10^{-5}	λ_{Ac}	9.88×10^{-6}	63
			9.81×10^{-6}	42

3.2. Example-2

In this Example, additional to the calculation the estimated parameters as in the previous example, it is necessary to calculate the dimensionless storativity coefficient. The reciprocal rate and reciprocal rate derivative data for this test are provided in Figure-10 and other relevant data are given below:

$q = 5$ Mscf/D $C = 0$ bbl/psi $s = 0$
$h = 200$ ft $T = 800$°R $\phi = 5\%$
$X_e = 3000$ ft $c_t = 1\times10^{-6}$ psi-1 $L = 50$ ft
$A_{cw}=1.2\times10^6$ ft^2 $\Delta m(P) = 1.2\times10^6$ psi^2/cp $\mu = 0.2$ cp

Solution. Taking into account the occurring flow regimes, the below parameters were read from Figure-10.

$t_L = 5.46\times10^{-6}$ hr $[t^*(1/q_g)']_L = 7.1\times10^{-7}$ D/Mscf
$t_{BL} = 9\times10^{-3}$ hr $[t^*(1/q_g)']_{BL} = 1.5\times10^{-5}$ D/Mscf
$t_{LM} = 4$ hr $[t^*(1/q_g)']_{LM} = 1.56\times10^{-4}$ D/Mscf
$t_{PSS} = 12.2$ hr $[t^*(1/q_g)']_{PSS} = 3.62\times10^{-4}$ D/Mscf
$t_{LPSSi} = 3.5\times10^4$ hr
$t_{MLPSSi} = 4.7\times10^5$ hr

Just as in Example-1, initially as the fracture permeability is unknown, the half-fracture length is calculated with Equation (52) using the pseudosteady-state period, generating a value of $y_e = 10467.96$ ft.

With the calculated value of y_e, the total matrix surface area draining into fracture system can be calculated by Equation (53) providing $A_{cm} = 62807760$ ft^2. Once calculated y_e, the fracture permeability can be calculated using the points of interception between the bilinear flow - matrix transient linear flow and matrix transient linear flow - pseudosteady-state flow with Equation (64), given as a result $k_f = 498.33$ md.

The dimensionless storativity ratio can be calculated using the point of interception between early linear flow regime with pseudosteady-state period by menas of Equation (59) given as result $\omega = 1.06\times10^{-2}$. Finally, the interporosity flow parameter can be calculated using the point of interception between matrix transient linear flow and pseudosteady-state flow with Equation (63) given as a result $\lambda_{Ac} = 4.75\times10^{-3}$. The other available equations were used to calculate the interporosity flow parameter and the dimensionless storativity coefficent. The input and calculated are shown in Table-2.

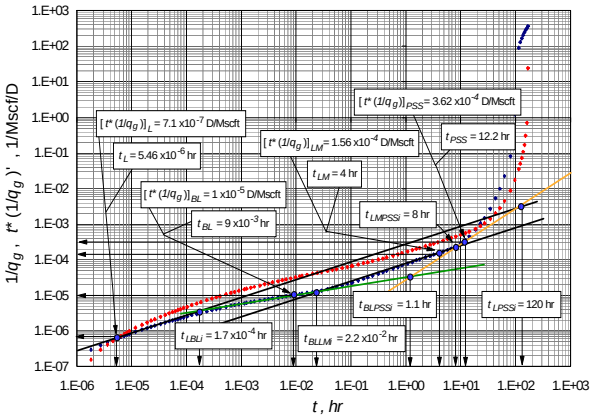

Figure-10. Log-log plot of the reciprocal rate and the reciprocal rate derivative vs. time for the Example-2.

Table-2. Summary of results for Example-2.

Parameter simulated		Parameter calculated		Eq.
y_e (ft)	10954.45	y_e (ft)	10467.96	52
A_{cm} (ft^2)	65726706.9	A_{cm} (ft^2)	62807760	53
k_f(md)	500	k_f(md)	498.33	64
ω	$1.\times10^{-2}$	ω	1.06×10^{-2}	59
			1.11×10^{-2}	28
			1.47×10^{-2}	55
λ_{Ac}	5×10^{-3}	λ_{Ac}	4.75×10^{-3}	63
			3.69×10^{-3}	33
			5.05×10^{-3}	42
			5.06×10^{-3}	56
			4.71×10^{-3}	61

3.3. Example-3

The reciprocal rate and reciprocal rate derivative for an example reported by Bello (2009) is presented in Figure-10. Other mportant data are given below:

$q = 3$ Mscf/D $C = 0$ bbl/psi $s = 0$
$h = 200$ ft $T = 660$°R $\phi = 15\%$
$X_e = 2000$ ft $c_t = 3.04\times10^{-4}$ psi-1 $L = 50$ ft
$A_{cw}=8\times10^5$ ft^2 $\Delta m(P) = 5.702\times10^8$ psi^2/cp
$\mu = 0.0224$ cp $k_f = 100$ md $k_m=1\times10^{-5}$ md

Solution. Linear flow regime, linear matrix flow regime and pseudosteady-sate period are presented in this test. The below data were read from Figure-11.

$t_L = 9.3\times10^{-4}$ hr $[t^*(1/q_g)']_L = 1.7\times10^{-8}$ D/Mscf
$t_{LM} = 1$hr $[t^*(1/q_g)']_{LM} = 2.9\times10^{-6}$ D/Mscf
$t_{PSS} = 4.5\times10^{4}$ hr $[t^*(1/q_g)']_{PSS} = 7\times10^{-4}$ D/Mscf
$t_{LPSSi} = 8\times10^{2}$ hr
$t_{MLPSSi} = 3\times10^{4}$ hr

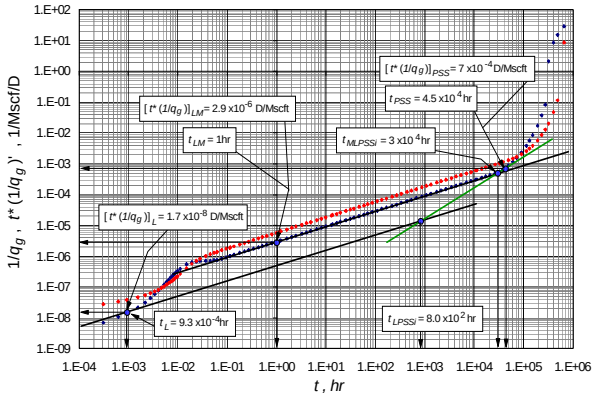

Figure-11. Log-log plot of the reciprocal rate and the reciprocal rate derivative vs. time for the Example 3.

Since the matrix permeability is known, the total matrix surface area draining into fracture system can be calculated by means of Equation (48) using the matrix transient linear flow regime, providing a value of $A_{cm} = 1.61\times10^{7}$ ft^2. The dimensionless storativity ratio can be calculated using the point of interception between early linear flow regime and the pseudosteady-state period with Equation (59). The resulting value of $\omega = 1.68\times10^{-3}$.

Table-3. Summary of results for Example-3.

Parameter simulated		Parameter calculated		Eq.
y_e (ft)	500	y_e (ft)	511	52
A_{cm} (ft^2)	1.6×10^{7}	A_{cm} (ft^2)	1.61×10^{7}	48
ω	1×10^{-3}	ω	1.68×10^{-3}	59
			1.09×10^{-3}	28
λ_{Ac}	3.84×10^{-4}	λ_{Ac}	4.3×10^{-4}	63
			3.87×10^{-4}	42

Then, interporosity flow parameter can be estimated with the point of interception between matrix transient linear flow regime and pseudosteady-period, t_{MLPSSi}, Equation (63), which provides $\lambda_{Ac} = 4.3\times10^{-4}$. Finally, the half-fracture length is calculated with Equation (52) using an arbitrary point read on the pseudosteady-state period. This provides a value of $y_e = 511$ ft. Other available relationships were used to calculate the flow capacity and the dimensionless storativity ratio. The input and calculated parameters are reported in Table-3.

4. CONCLUSIONS

- New expressions for interpretation reciprocal-rate transient tests shale gas formations are presented for rectangular reservoir geometry (slab) using characteristic points found on the reciprocal-rate derivative vs. time log-log plot. The interpretation equations are based on the linear dual porosity model proposed by El-Banbi 91998) to describe the hydraulically fractured shale gas reservoir system. The developed equations were successfully tested in simulated examples finding a very good agreement compared to the input data.
- The dimensionless storativity coefficient can be calculated only if the early linear flow regime is present because this affects only the behavior of the test to early times.
- The total matrix surface area draining into fracture system can be calculated from the period of seudosteady-state period and from the matrix transient linear flow if the matrix properties are known.
- The presence of all flow regimes in a test allows a complete characterization of the reservoir: calculation of fracture permeability, half-fracture length, total matrix surface area draining into fracture system, interporosity flow parameter and dimensionless storativity ratio. Otherwise, additional information is needed for a complete test interpretation.

ACKNOWLEDGEMENTS

The authors thank Universidad Surcolombiana and Universidad del Atlántico for providing financial support for the complement of this study.

REFERENCES

Al-Hussainy R., Ramey H.J. Jr. and Crawford P.B. 1966. The Flow of Real Gases through Porous Media. Journal of Petroleum Technology. 18(5): 624-636.SPE-1243-A-PA.

Anderson D.M., Nobakht M., Moghadam S. and Mattar L. 2010. Analysis of Production Data from Fractured Shale Gas Wells. Paper SPE 131787 presented at the SPE Unconventional Gas Conference, Pittsburgh, Pennsylvania, USA. 23-25 February.

Bello R.O. and Wattenbarger R. A. 2008. Rate Transient Analysis in Naturally Fractured Shale Gas Reservoirs. Paper SPE 114591-MS June. Texas A and M University.

Bello R.O. 2009. Rate Transient Analysis In Shale Gas Reservoirs With Transient Linear Behavior. PhD Dissertation. Texas A and M University.

Bennett C.O., Camacho-V. R.G., Reynolds A.C. and Raghavan R.1985. Approximate Solutions for Fractured

Wells Producing Layered Reservoirs. SPE J. 25(5): 729-742. SPE-11599-PA.

Brown M., Ozkan E. Raghavan R. and Kazemi H. 2011. Practical Solutions for Pressure-Transient Responses of Fractured Horizontal Wells in Unconventional Shale Reservoirs. SPE Reservoir Evaluation & Engineering. pp. 663-676.

Camacho-V., R.G., Raghavan R. and Reynolds A.C. 1987. Response of WellsProducing Layered Reservoir: Unequal Fracture Length. SPE Form Ev *al.* 2(1): 9-28. SPE-12844-PA.

Carlson E.S. and Mercer J.C. 1989. Devonian Shale Gas Production: Mechanisms and Simple Models. Paper SPE 19311 Eastern Regional Meeting, Morgantown, West Virginia, 24-27 October.

Cinco-Ley H. and Meng H.Z. 1988. Pressure Transient Analysis of Wells with Finite Conductivity Vertical Fractures in Double Porosity Reservoirs. Society of Petroleum Engineers. doi:10.2118/18172-MS., January 1.

Chen C.-C. and Raghavan R. 1997. A Multiply-Fractured Horizontal Well in a Rectangular Drainage Region. SPE J. 2(4): 455-465. SPE-37072-PA.

Escobar F.H., Castro J.R. and Mosquera J.S. 2014. Rate-Transient Analysis for Hydraulically Fractured Vertical Oil and Gas Wells. Journal of Engineering and Applied Sciences. ISSN 1819-6608. 9(5): 739-749.

El-Banbi A. H. and Wattenbarger R.A. 1998. Analysis of Linear Flow in Gas Well Production. Paper SPE 39972 presented at the SPE Gas Technology Symposium, Calgary, Alberta, Canada.

Escobar F.H., Montenegro L.M. and Bernal K.M. 2014. Transient-Rate Analysis For Hydraulically-Fractured Gas Shale Wells Using The Concept Of Induced Permeability Field. Journal of Engineering and Applied Sciences. ISSN 1819-6608. 9(8): 1244-1254.

Escobar F.H., Bernal K.M. and Olaya-Marin G. 2014. Pressure and Pressure Derivative Analysis for Fractured Horizontal Wells in Unconventional Shale Reservoirs Using Dual-Porosity Models in the Stimulated Reservoir Volume. Journal of Engineering and Applied Sciences. Paper sent to request publication.

Fuentes-Cruz G., Gildin E. and Valko P. 2014. Analyzing Production Data from Hydraulically Fractured Wells: the Concept of Induced Permeability Field. SPE Formation Evaluation. pp. 1-13.

Ge J. and Ghassemi A. 2011. Permeability Enhancement in Shale Gas Reservoirs after Stimulation by Hydraulic Fracturing. Paper AR11-514 presented at the Rock Mechanics / Geomechanics Symposium, San Francisco, CA.

Mayerhofer M.J., Lolon E.P., Youngblood J.E. and Heinze J.R. Integration of Microseismic Fracture Mapping Results with Numerical Fracture Network Production Modeling in the Barnett Shale. Paper SPE 102103 presented at the 2006 Annual Technical Conference and Exhibition, San Antonio, Texas, 24-27 September.

Ozkan E., Ohaeri U. and Raghavan R. 1987. Unsteady Flow to a Well Produced at a Constant Pressure in a Fractured Reservoir. Society of Petroleum Engineers. doi:10.2118/9902-PA. June 1.

Palmer I.D., Moschovidis Z.A. and Cameron J.R. 2007. Modeling Shear Failure and Stimulation of the Barnett Shale after Hydraulic Fracturing. Paper SPE 106113 presented at the SPE Hydraulic Fracturing Technology Conference, College Station, Texas, U.S.A.

Serra K., Reynolds A. C. and Raghavan R. 1983. New Pressure Transient Analysis Methods for Naturally Fractured Reservoirs (includes associated papers 12940 and 13014). Society of Petroleum Engineers. doi:10.2118/10780-PA. December 1.

Spivey J. P. and Semmelbeck M. E. 199. Forecasting Long-Term Gas Production of Dewatered Coal Seams and Fractured Gas Shales. Society of Petroleum Engineers. doi:10.2118/29580-MS. January 1.

Tiab D. 1993. Analysis of Pressure and Pressure Derivative without Type-Curve Matching: 1- Skin and Wellbore Storage. Journal of Petroleum Science and Engineering. 12: 171-181.

Van Everdingen and Hurst W. 1949. The Application of Laplace Transformation to Flow Problems in Reservoirs. Petroleum Transactions, AIME. pp. 305-324.

Wattenbarger R.A., El-Banbi A.H., Villegas M.E. and Maggard J. B. 1998. Production Analysis of Linear Flow into Fractured Tight Gas Wells. Paper SPE 39931 presented at the SPE Rocky Mountain Regional/Low Permeability Reservoirs Symposium, Denver, Colorado.

Warren J. E. and Root P. J. 1963. The Behavior of Naturally Fractured Reservoirs. Society of Petroleum Engineers. doi:10.2118/426-PA. September.

Watson A. T., Gatens J. M., Lee W. J. and Rahim Z. 1990. An Analytical Model for History Matching Naturally Fractured Reservoir Production Data. Society of Petroleum Engineers. doi:10.2118/18856-PA. August 1

APPENDIX-A. GOVERNING EQUATIONS FOR PRESSURE DERIVATE GAS FLOW

A.1. Linear early flow regime

The dimensionless equation representing the first linear flow regime is given by:

$$t_{DL} * (1/q_D)'_L = 2\left(\frac{\pi t_{DA}}{\omega}\right)^{\frac{1}{2}} \quad (A.1)$$

Once the dimensionless terms given by Equations (5) and (12) are plugged into Equation (A.1), the fracture permeability can be solved for:

$$k_f = \frac{6700.68\, t_L}{(\phi\mu c_t)_{f+m}\, \omega}\left(\frac{q_g T}{A_{cw}\left[t * \Delta m(P')\right]}\right)^2 \quad (A.2)$$

From the above equation it is possible to know the value of the dimensionless storativity coefficient:

$$\omega = \frac{6700.68\, t_L}{(\phi\mu c_t)_{f+m}\, k_f}\left(\frac{q_g T}{A_{cw}\left[t * \Delta m(P')\right]}\right)^2 \quad (A.3)$$

A.2. Bilinear flow regime

The general equation describing this flow regime, for the bilinear model in dimensionless terms is:

$$t_D * (1/q_D)'_{MLL} = \frac{2.28075}{\lambda^{0.25}} (t_{DA})^{0.25}_{BL} \quad (A.4)$$

It is possible to obtain from Equation (A.4) equations for calculating k_f and λ, respectively,

$$k_f = \left(\frac{4009.76}{A_{cw}}\right)\left(\frac{q_g T}{\left[t * m(P')\right]}\right)^{1/0.75}\left(\frac{t}{(\phi\mu c_t)_{f+m}\, \lambda_{AC}}\right)^{0.33} \quad (A.5)$$

$$\lambda_{AC} = \left(\frac{6.54\text{x}10^{10}\, t}{(\phi\mu c_t)_{f+m}}\right)^{0.33}\left(\frac{q_g T}{\left[t * m(P')\right] k_f^{0.75}\, A_{cw}^{0.75}}\right)^{1/0.25} \quad (A.6)$$

A.3. Matrix transient linar model

The dimensionless governing equation representing the second linear flow is given by:

$$t_{DL} * (1/q_D)'_L = 2\left(\frac{3\pi t_{DA}}{\lambda_{AC}}\right)^{\frac{1}{2}}\left(\frac{1}{y_{De}}\right) \quad (A.7)$$

Once the dimensionless terms given by Equations (5) and (12) are plugged into Equation (A.1), the fracture permeability can be solved for:

$$k_f = \frac{60306.44213\; t_{Lt}\, A_{cw}}{(\phi\mu c_t)_{f+m}\; \lambda_{AC}}\left(\frac{q_g T}{y_e\left[t * \Delta m(P')\right]}\right)^2 \quad (A.8)$$

From the above equation it is possible to know the value of the interporosity flow parameter:

$$\lambda_{AC} = \frac{60306.44213\; A_{cw}\, t_{Lt}}{(\phi\mu c_t)_{f+m}\, k_f}\left(\frac{q_g T}{y_e\left[t * \Delta m(P')\right]}\right)^2 \quad (A.9)$$

A.4. Homogeneus transient linear model

The dimensionless governing equation for the second linear flow is:

$$t_{DL} * (1/q_D)'_{Lh} = \left(2\pi t_{DH}\right)^{\frac{1}{2}} \quad (A.10)$$

Once the dimensionless terms given by Equations (5) and (12) are plugged into Equation (A.7), the fracture permeability can be solved for:

$$k_f = \frac{6700.68\; t_{Lt}}{(\phi\mu c_t)_{f+m}}\left(\frac{q_g T}{A_{cw}\left[t * \Delta m(P')\right]}\right)^2 \quad (A.11)$$

A5. Intersection Points

Intersection point between Early Linear and Bilinear flow

This intersection point used for obtaining the interporosity flow parameter:

$$\lambda_{AC} = \frac{k_f t_{LBLi}\, \omega^2}{22130.91\; (\phi\mu c_t)_{f+m}\, A_{cw}} \quad (A.10)$$

Intersection point between Second Linear and Bilinear flow regimes

This intersection point also provides the interporosity flow parameter:

$$\lambda_{AC} = \frac{k_f t_{LBLi}}{569632.11\, y_e^{\,2} (\phi\mu c_t)_{f+m}\, A_{cw}} \quad (A.11)$$

Nomenclature

A_{cm}	Total matrix surface area draining into fracture ystem, ft2
A_{cw}	Well-face cross-sectional area to flow, ft^2
B	Liquid formation volume factor, rB/STB
B_{gi}	Formation volume factor at initial reservoir pressure, rcf/scf
c_t	Liquid total compressibility, psi^{-1}
c_{ti}	Total compressibility at initial reservoir pressure, psi-1
$f(s)$	Relation used in Laplace space to distinguish matrix geometry types
h	Reservoir thickness, ft
$I_o(x)$	Modified Bessel function of first kind, zero order
$I_1(x)$	Modified Bessel function of first kind, first order
$J_o(x)$	Bessel function of first kind, zero order
k	Homogeneous reservoir permeability, md
k_f	Bulk fracture permeability of dual porosity models, md
k_m	Matrix permeability, md
k_V	Vertical permeability, md
k_H	Horizontal permeability, md
l	Half of fracture spacing, ft
l^{-1}	Inverse Laplace space operator
L	General fracture spacing, ft
L_w	Horizontal well length, ft
$m(p)$	Pseudopressure (gas), psi^2/cp
p_i	Initial reservoir pressure, psi
p_{wf}	Wellbore flowing pressure, psi
q_g	Gas rate, Mscf/day
Q	Cumulative production, STB
r_w	Wellbore radius , ft
s	Laplace space variable
t	Time, days
t_D	Dimensionless time coordinate
t_{DAc}	Dimensionless time based on A_{cw} and k_f (rectangular geometry, dual porosity)
t_{DAch}	Dimensionless time based on A_{cw} and k (rectangular geometry, homogeneous)
t_{DAcm}	Dimensionless time based on matrix A_{cm} and k_m (rectangular geometry)
t_{Drw}	Dimensionless time (radial definition) based on wellbore radius
T	Absolute temperature, ^oR
x_e	Drainage area width (rectangular geometry), ft
y_e	Drainage area half-length (rectangular geometry), ft geometry), ft
y_{De}	Dimensionless reservoir length (rectangular geometry)
z	Coordinate, z-direction (matrix)
z_D	Dimensionless coordinate, z-direction

Greeks

γ	Specific gravity
λ	Dimensionless interporosity parameter
ϕ	Porosity, fraction
μ	Viscosity, cp
ω	Dimensionless storativity ratio

Suffices

D	Dimensionless
DA	Dimensionless based on drainage area
sc	Standard conditions
L	Early Linear flow
BL	Bilinear flow
LM	Matrix Transient Linear flow
h	Linear Homogeneuos flow
LBLi	Early Linear flow - Bilinear flow intercepted
BLLMi	Bilinear flow - Matrix Transient Linear flow intercepted
LPSSi	Early Linear flow - Pseudosteady-State flow intercepted
BLPSSi	Bilinear flow - Pseudosteady-State flow intercepted
LMPSSi	Matrix Transient Linear flow- Pseudosteady-State flow intercepted
PSS	Pseudosteady-State flow